IEEE Access
Multidisciplinary ⋮ Rapid Review ⋮ Open Access Journal

Received September 29, 2020, accepted October 10, 2020, date of publication October 21, 2020, date of current version November 2, 2020.

Digital Object Identifier 10.1109/ACCESS.2020.3032705

Power Management Strategy Based on Adaptive Neuro Fuzzy Inference System for AC Microgrid

HESHAM M. FEKRY[1], AZZA AHMED ELDESOUKY[2], AHMED M. KASSEM[3], AND ALMOATAZ Y. ABDELAZIZ[4], (Senior Member, IEEE)

[1]Department of Electrical Engineering, Egyptian Propylene and Polypropylene Company, Port Said 42511, Egypt
[2]Department of Electrical Power, Faculty of Engineering, Port Said University, Port Fouad 42526, Egypt
[3]Department of Electrical Engineering, Faculty of Engineering, Sohag University, Sohag 82524, Egypt
[4]Faculty of Engineering and Technology, Future University in Egypt, Cairo 11835, Egypt

Corresponding author: Hesham M. Fekry (eng.heshamfekry@gmail.com)

ABSTRACT Microgrids (MGs) have been widely implemented as they increase the efficiency and resiliency of electrical networks. However, the uncertain nature of renewable energy resources (RERs) integrated into the MGs usually results in different technical problems. System stability, the most challenging problem, can be achieved via a robust power management strategy (PMS) of the MG. This paper introduces a PMS based on adaptive neuro fuzzy inference system (ANFIS) for AC MG consisting of a diesel generator (DG), a double fed induction generator (DFIG) driven by a wind turbine (WT) and a solar photovoltaic (PV) panel. The proposed strategy aims to achieve MG power balance, decrease DG fossil fuel to minimum consumption, keep the MG voltage stability and finally tracking the maximum power point (MPP) of each RER. Metaheuristic optimization techniques; including genetic algorithm (GA) and particle swarm optimization (PSO), are employed to train the ANFIS to accomplish the desired objectives and fulfill the generation/consumption balance. The proposed AC MG with the PMS is simulated by the MATLAB/Simulink software in order to analyze the system performance under different climatic conditions. The simulation results under symmetrical and asymmetrical electrical faults validated the effectiveness of the proposed strategy.

INDEX TERMS Microgrid, renewable energy resources, power management strategy, voltage stability, adaptive neuro fuzzy inference system, double fed induction generator, genetic algorithm, particle swarm optimization.

NOMENCLATURE

C_P	efficiency coefficient of the wind turbine.
G	solar irradiation.
I_g	PV generator current.
L_r	DFIG rotor leakage inductance.
L_s	DFIG stator leakage inductance.
P_{DG}	diesel generator output active power.
P_{GSC}	grid side converter active power.
$P_{mec.}$	diesel generator input mechanical power.
P_{pv}	PV generator active power.
P_r	DFIG rotor active power.
P_s	DFIG stator active power.
P_ω	extracted wind power.
Q_S	DFIG stator reactive power.
R	rotor radius.
R_s	DFIG stator resistance.
R_r	DFIG rotor resistance.
s	slip.
t	time interval.
V_g	PV generator voltage.
v	wind speed.
ω_r	rotor angular frequency.
ω_s	synchronously rotating reference frame angular velocity.
ω_{slip}	slip angular frequency.
ω_t	turbine rotational speed.
β	blade pitch angle.
λ	tip-speed ratio.
ρ	air density.

The associate editor coordinating the review of this manuscript and approving it for publication was Canbing Li.

I. INTRODUCTION

Today, as the world population is drastically increasing, the excessive consumption of fossil fuels has led to higher levels

of pollution, greenhouse gas emissions and perceptible climatic changes that pose a dangerous threat to the anthropological and natural ecosystems [1], [2]. These harmful influences have highlighted the need for renewable energy resources (RERs) as safe and clean forms for power generation [3]. Meanwhile, Microgrids (MGs) are considered an effective way of managing the RERs integration on both the distribution system level and the user level [4]. The use of MGs allows the RERs to operate independently during main grid failure. This in turn helps efficient transformation of the passive network into an active one, bidirectional and controlled power flow management, reliable and continuous supply, power quality enhancement, and clean environment [3]. They can offer an affordable and effective means of enhancing the energy supply of the continuously growing communities [2], [4]. In the near future, electricity generation networks will need to accommodate RERs on larger scales and facilitate their connection with major grids at suitable locations [5].

Undoubtedly, the well-designed power management (PM) is essential to a functional MG as the distribution feature renders their control structure greatly different from that of the traditional/central power plants. Many demonstration projects and laboratory testing systems have been designed to verify one or more specified PM performances [6]. In [7], the PM for a MG consisting of a photovoltaic (PV), a wind turbine (WT), a distributed generator, and a battery bank with linear and non-linear loads was achieved through the utilization of the adaptive neuro fuzzy inference system (ANFIS) with elephant herd optimization (EHO) algorithm. The authors in [8] introduced a PM system for PV-battery-hydro based MG capable of regulating the frequency and voltage of the MG and load leveling and organized the active power circulating during battery charging and discharging. Similarly, in [9], a PV/battery hybrid distributed power generation system was proposed with a power management strategy (PMS) of only one integrated three-port power converter. In [10], an efficient PMS for a small-scale hybrid wind-solar-battery RER based MG was designed to maintain the MG power balance and accommodate the different variations in the RERs and the load demand. In [11], an improved PMS of a hybrid direct current DC MG system consisting of a PV cell, WT generator, battery energy storage, fuel cell and an electrolyzer was adopted. The transient response of the voltage was improved using Takagi–Sugeno fuzzy control.

A MG including diesel, battery storage, and solar plants was proposed in [12]. An effective PM was achieved through a time domain signal processing approach to filter the fluctuating output power of the solar plant. The study in [13] presented a PMS of a MG based on a modified Tribe- particle swarm optimization (PSO), a demand response program and a power scheduling approach. In [14], the authors used a model predictive control theory as the mathematical framework and a fuzzy prediction interval model as the prediction model representing both nonlinear dynamic behavior and uncertainty in the RERs.

Based on the above studies, it is noticeable that wind and PV are the two leading RERs that have come to the forefront of the scientific and experimental research in the field of clean renewable power generation [15], [16]. However, the intermittent and stochastic natures of them have complicated their use and therefore, it is better to be merged with conventional diesel generator (DG). Studies have shown that the reliability of a hybrid wind and solar PV system is twice as much as for either technology used alone [17]. These combined systems fulfill the energy security and stability as well as increased power quality and whole-system efficiency [18].

In our study, a PMS based on ANFIS is proposed for a MG consisting of a double fed induction generator (DFIG) driven by a WT and a solar PV panel as a hybrid renewable energy system in combination with a DG. The implementation of ANFIS controller is promoted for various reasons. The learning ability of artificial neural network (ANN) eliminates the basic problems in fuzzy system design, which provides the parameter optimization ability with a high degree of tolerance to uncertainty and possible system disturbances. Therefore, it can deal with any unexpected changes in the environmental conditions even if not predefined or previously occurred. Moreover, it can easily correlate the inhomogeneous inputs and calculate the output without complex mathematical models. It continuously extends its base of knowledge through the addition of new rules which makes the system upgrading easier and faster with no need for long shutdowns [19]. To achieve optimum MG energy operation and control, metaheuristic optimization algorithms such as the genetic algorithm (GA) and particle swarm optimization (PSO) are further proposed for training the ANFIS [20].

Depending on the climatic changes, different input variables are collected to the ANFIS. These are the wind speed, the solar irradiation and the ambient temperature. The output is the mechanical power of the DG to optimally dispatch the required generated power to overcome the uncertainty of the RERs. Different case studies depending on the weather conditions and the state of the network are studied. In this work, the PV is used to drive the rotor of the DFIG with different scenarios depending on the density of the solar irradiation. The main contributions of this work can be summarized as:

1- A smart PMS for a MG that blends renewable and traditional resources based on ANFIS is proposed.
2- GA and PSO as metaheuristic optimization algorithms are presented for ANFIS's parameters enhancement to improve the system performance.
3- The climatic parameters are the inputs of the proposed ANFIS to deduct the most accurate mechanical power of the DG, making the system more stable and efficient.
4- The DFIG is often operating on sub-synchronous mode in this work, promoting the connection of the PV terminals to DC link to save the use of a separate inverter between the PV and the MG load bus which, in turn, saves money and ensures that the resulting voltage and currents are smoothed.

5- Different case studies are performed considering the different climatic and temporary fault conditions in order to validate the effectiveness of the proposed system control.

Accordingly, this paper is arranged as follows: In section II, the system used is described including the description of the proposed ANFIS structure with different optimizations algorithms and the model of each energy resource. Section III presents the simulation results and discussion. Finally, the conclusions are introduced in section IV.

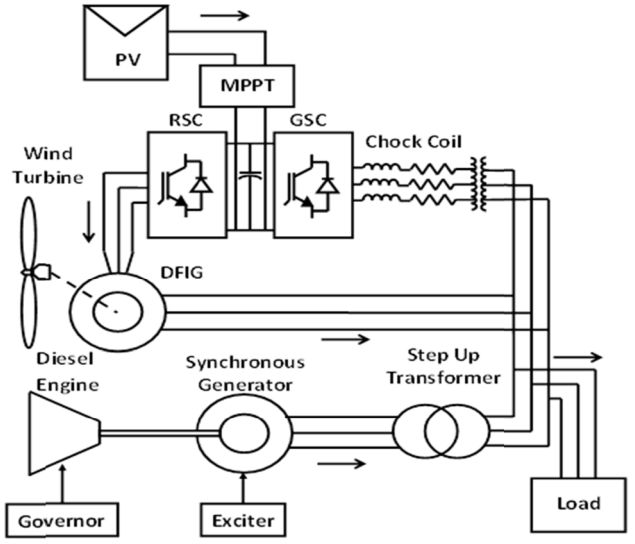

FIGURE 1. The schematic diagram of the proposed hybrid power system in MG.

II. ISOLATED MG DESCRIPTION

The schematic diagram of the proposed MG is shown in Fig.1. The MG is formed of three different power sources, two of them are renewable sources (DFIG driven by a WT and PV) and the third source is a traditional DG. The MG is responsible for continuously supplying a two-megawatt residential load. The DFIG stator is directly connected to the grid whereas the PV is directly connected to a DC bus through a maximum power point (MPP) boost circuit to feed the DFIG rotor through the rotor side converter (RSC) and also supply the grid occasionally through grid side converter (GSC) via a chock coil. Meanwhile, the DG stator is coupled with the mentioned grid through a step up power transformer that raises the voltage from 400 V to 575 V as the main voltage of MG and load.

The PMS of the proposed system should be capable of executing the following objectives:

1. Achieving the MG voltage stability.
2. Keeping power balance in the MG.
3. Decreasing the fuel consumption of the DG to a minimum value.
4. Tracking the MPP of wind and PV resources.

The first and fourth objectives are carried out by the own design control for each of DFIG driven by WT, PV, and DG as briefly discussed later on. For the second and third objectives, they are achieved through a control strategy that predicts the generated power output of the renewable sources and accordingly calculates the needed mechanical power input. This accurately determines the minimum amount of the diesel engine fuel required to complete the two megawatt of the mentioned residential load and to achieve the whole-system power balance.

In general, the ANFIS is an intelligent system based on learning and combines data processing ability of ANN and inference capability of Takagi-Sugeno fuzzy inference system. The ANFIS controller uses the ''IF–THEN'' rules according to the learning algorithms to decrease the output error based on the training data sets [21], [22].

The main ANFIS structure consists of five functional blocks (rule base, database, a decision making unit, a fuzzyfication and a defuzzyfication interface modules). The classic hybrid learning algorithm (HLA) for ANFIS uses a combination of gradient descent (GD) and least squares estimator (LSE) in a two-pass parameter update process [23].

The design of the proposed ANFIS comprises three inputs and one output. The first input is the wind speed representing the output power generated from the DFIG driven by WT. The second and the third inputs are the solar irradiation and ambient temperature as indications of the output power extracted from PV generator. The ANFIS output is the expected mechanical power that should be dispatched to DG to complete the power required to balance the residential load as previously illustrated. 385 training samples are used to train the proposed ANFIS, GA-ANFIS and PSO-ANFIS controllers. Table 1 presents ten random training samples. The internal structure of the proposed ANFIS controller is displayed in Fig. 2. Each input has a triangular membership number of three while the number of rules is twenty seven.

TABLE 1. Ten random samples from ANFIS training samples.

Input 1 Wind Speed (m/s)	Input 2 Solar Irradiation (W/m^2)	Input 3 Ambient Temp. (c°)	output Diesel Mech. Power (W)
9.6	1000	40	879600
12	600	30	611900
7.2	700	15	1801250
8.4	800	35	1206500
9.6	300	25	1343400
12	200	15	871800
8.4	400	20	1457300
7.2	100	30	1382400
8.4	0	35	1725000
12	900	25	404000

Additionally, the results of the ANFIS are further compared to those of (GA-ANFIS), and (PSO-ANFIS). The validity of the three ANFIS controllers is verified by the simulation results carried out using MATLAB/ Simulink environment. Table 2 displays the applied parameters of the GA and PSO.

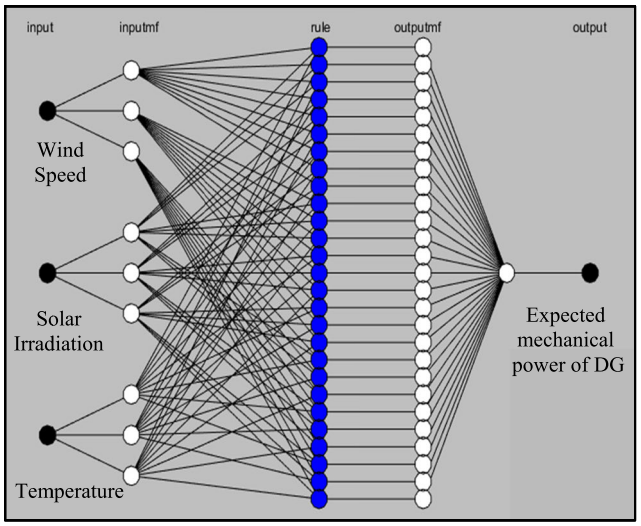

FIGURE 2. The internal structure of the proposed ANFIS controller trained by HLA algorithm.

TABLE 2. The applied parameters for the proposed GA and PSO.

GA Parameters	PSO Parameters
Population Size: 20	Population Size: 20
Maximum Number of Iterations: 1000	Maximum Number of Iterations: 1000
Crossover Percentage: 0.4	Inertia Weight: 1
Mutation Percentage: 0.7	Inertia Weight Damping Ratio: 0.99
Mutation Rate: 0.15	Personal Learning Coefficient: 1
Selection Pressure: 8	Global Learning Coefficient: 2
Gamma: 0.7	

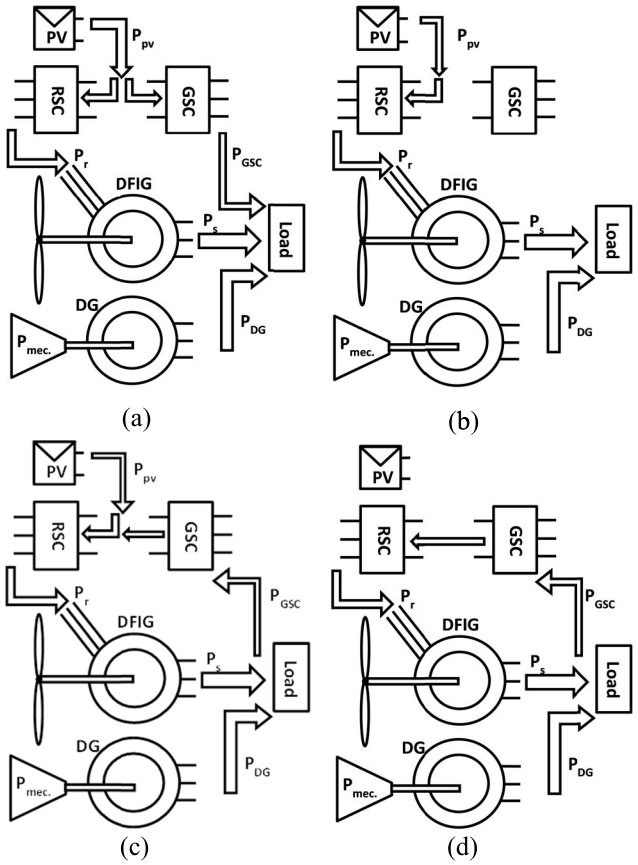

FIGURE 3. The main power flow segments of the proposed hybrid power system during most of the day: (a) PV supplies both of the DFIG rotor power and the MG load directly during high solar irradiation. (b) PV supplies the DFIG rotor power only when the sunlight is light. (c) The DFIG rotor power is supplied by the PV and the MG when the solar irradiation becomes weaker. (d) The DFIG rotor power supplied only by the MG during solar irradiation fading.

For the proposed system, the torque speed characteristic of the WT, as will be displayed later, drives the DFIG to run always in sub-synchronous operation mode even in the case of high or low wind speeds that may be expected in the proposed geographical site of installation. This can be quite advantageous as all the mechanical power output of the WT along with any electrical power received from the rotor will be exploited by the DFIG stator.

The hybrid power system concept is specifically applied in this work to avoid any sudden disturbances in the MG resulting from probable failure in the renewable components. The DG is always in service supplying the grid and the precise amount of its contribution is determined according to the proposed ANFIS controller as previously discussed.

Fig. 3 summarizes the main power flow segments of the proposed hybrid power system during most of the day. During the maximum solar irradiation, a part of the PV power output supplies the DFIG rotor and the rest is fed to the grid through the GSC which acts as an inverter. The power rating of the used PV array at the maximum expected solar irradiation and minimum expected ambient temperature is chosen to be more than the highest DFIG rotor power consumption according to the following relation:

$$P_r = sP_s \tag{1}$$

where P_r and P_s are the DFIG rotor and stator power, respectively and s is the slip.

When the solar irradiation declines, the PV power is decreased and feeds the rotor only. In case that the sunlight becomes even feebler, the PV cannot even feed the rotor alone and the GSC acts as a converter contributing to the rotor supply with an amount of power from the MG through the DC bus. Finally, when the solar irradiation fades away, the rotor is totally fed by the MG.

A. THE PV

The PV generator has a nonlinear voltage current characteristic based on solar irradiation and ambient temperature. It can be expressed from the following formula:

$$V_g = \frac{1}{A_g} \ln\left[\frac{GI_{phg} - I_g + I_{og}}{I_{og}}\right] - I_g R_{sg} \tag{2}$$

where V_g & $I_g$are the PV generator voltage and current, respectively; $A_g = \Lambda/Ns$ is the PV generator constant;

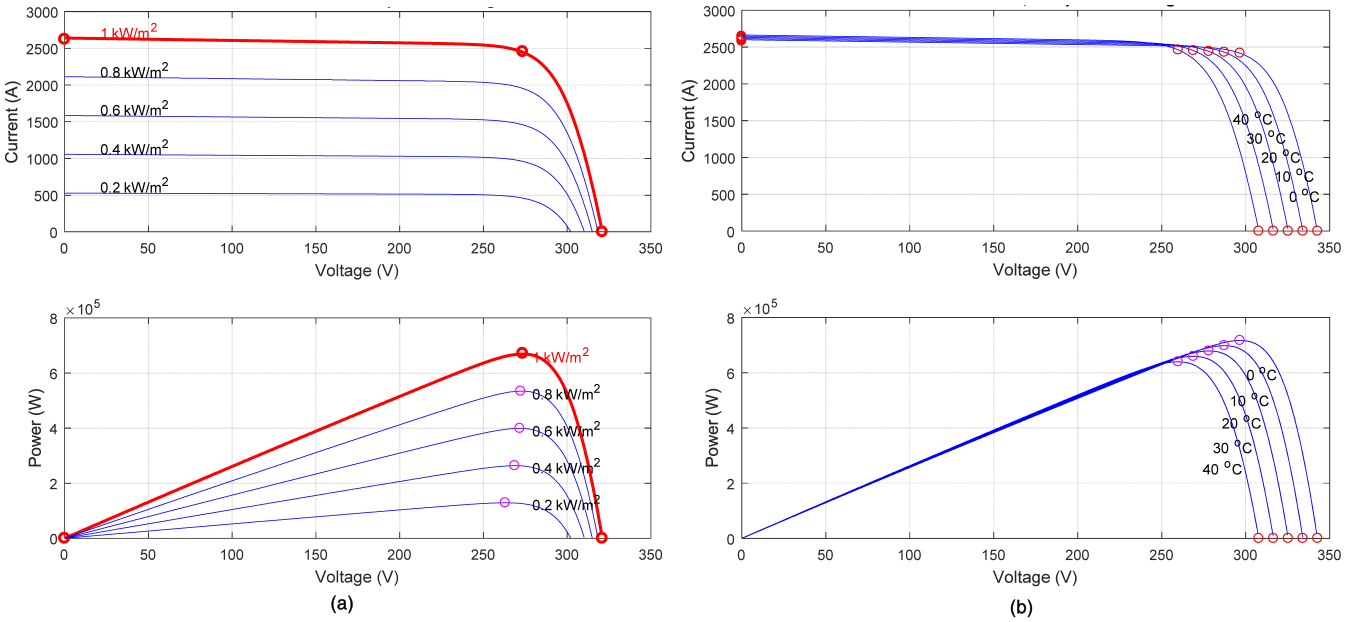

FIGURE 4. PV characteristics. (a) The current and power versus PV voltage characteristics with solar irradiation changing. (b) The current and power versus PV voltage characteristics with ambient temperature changing.

Λ =q/(ε×Z×U), is the solar cell constant; q= 1.602 × 10^{-19} C. is the electron charge; Z= 1.38 × 10^{-23} J/K is Boltzman constant; U= 298.15; K is the absolute temperature; ε =1.1 is the completion factor; $R_{sg} = R_s \times (N_s/N_p)$ is the PV generator series resistance; N_s is the series connected solar cells; N_p is the parallel paths; R_s is the series resistance per cell; $I_{phg} = \mathrm{I_{ph}} \times N_p$ is the insolation-dependent photo current of the PV generator; $\mathrm{I_{ph}} = 4.8$ A is the photo current per cell; $I_{og} = I_o \times N_p$ is the PV generator reverse saturation current; $\mathrm{I_o}$ =2.58e^{-5} A is the reverse saturation current per cell; G is the solar insolation in per unit, and 1.0 per unit of G=1000 W/m^2 [24].

Fig. 4 displays the characteristics of the drawn current and output power versus the PV terminal voltage along the changing of both the solar irradiation and the ambient temperature for the used PV panel. The output power and the short circuit current increase proportionally as the solar irradiation increases whereas they decline as the ambient temperature decreases and vice versa. The characteristics clearly indicate that there is a unique point at which the PV can produce the maximum power at each certain solar irradiation and temperature. Many methods are implemented to track this maximum power operating point by changing the pulse width modulation duty cycle of a boost or buck boost circuit installed on the terminal of PV panel. In this work, the traditional P&O algorithm is used. This algorithm depends on the comparison between the recent PV power output (P_n) and the previous (P_{n-1}) until the difference between them,ΔP, reaches zero. This method has the drawback of the slow response to the irradiation and temperature changes, however it is still the simplest method [25]. The proposed PV array type is SunPower SPR 305E-WHT-D built from 440 parallel strings and each string consists of 5 series modules with attached MPP tracking boost circuit. The philosophy of PV power rating selection, as displayed in the proposed array technical specifications, Table 3, is to determine the sufficient power that should supply the DFIG for optimum running at 1000 W/m^2 solar irradiation and 25 c° ambient temperature during all expected wind speeds and in case of any excess power, it feeds the grid directly.

TABLE 3. The main technical specifications of the used PV array at 1000W/m^2 solar irradiation, 25 c° ambient temperature.

Description	Specification
Array type	SPR 305E-WHT-D
Rated maximum power	671500 W
Voltage at maximum power	273.5 V
Current at maximum power	2455 A
Open circuit voltage	321 V
Short circuit current	2622 A

B. THE DFIG DRIVEN BY WT

The wind energy conversion system transforms the wind kinetic energy into mechanical energy by means of the aerodynamic forces that produce lift on the rotor shaft blades. It can be calculated as [26]:

$$P_\omega = \frac{1}{2}\rho\pi R^2 v^3 C_P(\lambda, \beta) \tag{3}$$

where P_ω is the extracted wind power, ρ is the air density (1.225 kg/m^3), R is the rotor radius, v is the wind speed and C_P is the efficiency coefficient of the turbine which is the

function of the tip-speed ratio λ and the blade pitch angle β. The tip-speed ratio λ is expressed as:

$$\lambda = \frac{\omega_t R}{v} \tag{4}$$

where ω_t is the turbine rotational speed.

The DFIG is the most commonly used WT-driven generator especially when high power ratings are needed as intended in the proposed system. This technology has been widely implemented due to its numerous advantages. The DFIG-based WTs are able to capture more wind energy and support the grid with large reactive power during short disturbance events. However, DFIG is very sensitive to the possible grid faults [27], [28]. It has three modes of operation categorized according to the operating rotational speed and the rotor power direction. In the "super-synchronous" mode, the operating speed is always above the synchronous speed and the rotor supplies a part of the generated power. The second mode is called "synchronous" mode, where the operating speed is the synchronous speed and the rotor does not supply or receive any AC power but receives a DC power to act as an exciter. The third is the "sub-synchronous" mode, where the operating speed is always below the synchronous speed and the rotor receives a part of the generated power.

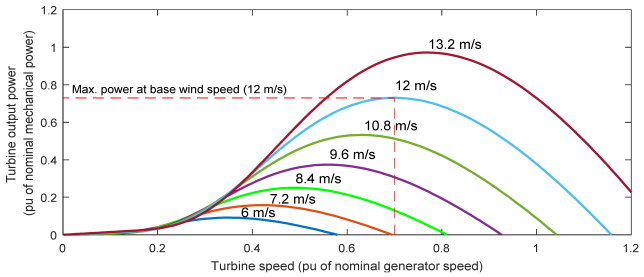

FIGURE 5. The power characteristic of the used WT.

The power characteristic curve between the rotational speed and the output power for any WT has a MPP that changes according to the wind speed. Therefore, the MPP tracking curve specifies the reference power for the control system of the driven electrical generator according to the actual speed of the WT [29], Fig. 5. The figure also shows that the proposed turbine is designed to produce always the maximum power at speeds less than the DFIG synchronous speed even with different wind speeds. The sub-synchronous operation mode of the DFIG is the part assigned to our study where the wind speed is chosen to be ranged from 13.2 to 6 m/s. Table 4 summarizes the main technical specifications of the proposed wind energy system.

In this work, the stator voltage oriented control (SVOC), Fig. 6, is used to represent the mathematical model of the DFIG throughout sets of equations to infer the stator active and reactive powers in terms of rotor d-q axis currents as displayed in the following voltage and flux sets of

TABLE 4. The main technical specifications of WT and DFIG.

Description	Specification
Turbine nominal mechanical power	1.5 MW
Base wind speed	12 m/s
Maximum power at base wind speed	0.73 pu of nominal mechanical power
Base rotational speed	0.7 pu of base generator speed
DFIG rated capacity	1.67 MVA
Nominal stator voltage	575 V
Nominal frequency	50 Hz
Poles pairs number	3
DC bus voltage	1200 V
Stator resistance & inductance	0.023 & 0.18 pu
Rotor resistance & inductance	0.016 & 0.016 pu
Mutual inductance	2.9 pu
Inertia constant	0.095 s
Friction factor	0.054 pu

equations [29]:

$$V_{ds} = R_s I_{ds} - \omega_s \psi_{qs} + \frac{d\psi_{ds}}{dt} \tag{5}$$

$$V_{qs} = R_s I_{qs} + \omega_s \psi_{ds} + \frac{d\psi_{qs}}{dt} \tag{6}$$

$$V_{dr} = R_r I_{dr} - \omega_{slip} \psi_{qr} + \frac{d\psi_{dr}}{dt} \tag{7}$$

$$V_{qr} = R_r I_{dr} + \omega_{slip} \psi_{dr} + \frac{d\psi_{qr}}{dt} \tag{8}$$

$$\psi_{ds} = L_s I_{ds} + L_m I_{dr} \tag{9}$$

$$\psi_{qs} = L_s I_{qs} + L_m I_{qr} \tag{10}$$

$$\psi_{dr} = L_r I_{dr} + L_m I_{ds} \tag{11}$$

$$\psi_{qr} = L_r I_{qr} + L_m I_{qr} \tag{12}$$

$$L_s = L_{is} + L_m \tag{13}$$

$$L_r = L_{ir} + L_m \tag{14}$$

where:

V_{ds} & V_{qs}: The d- q axis stator voltages, respectively;
V_{dr} & V_{qr}: The d-q axis rotor voltages, respectively;
ψ_{ds} & ψ_{qs}: The d-q axis stator flux linkages, respectively;
ψ_{dr} & ψ_{qr}: The d-q axis rotor flux linkages, respectively;
I_{ds} & I_{qs}: The d-q axis stator currents, respectively;
I_{dr} & I_{dr}: The d-q axis rotor currents, respectively;
R_s & R_r: The stator and rotor resistances, respectively;
L_m : The magnetizing inductance;
L_s : The stator leakage inductance;
L_r : The rotor leakage inductance;
L_{is} : The stator self-inductance;
L_{ir} : The rotor self-inductance,
ω_s : The synchronously rotating reference frame angular velocity;
ω_r : The rotor angular frequency;
$\omega_{slip} = \omega_s - \omega_r$: The slip angular frequency.

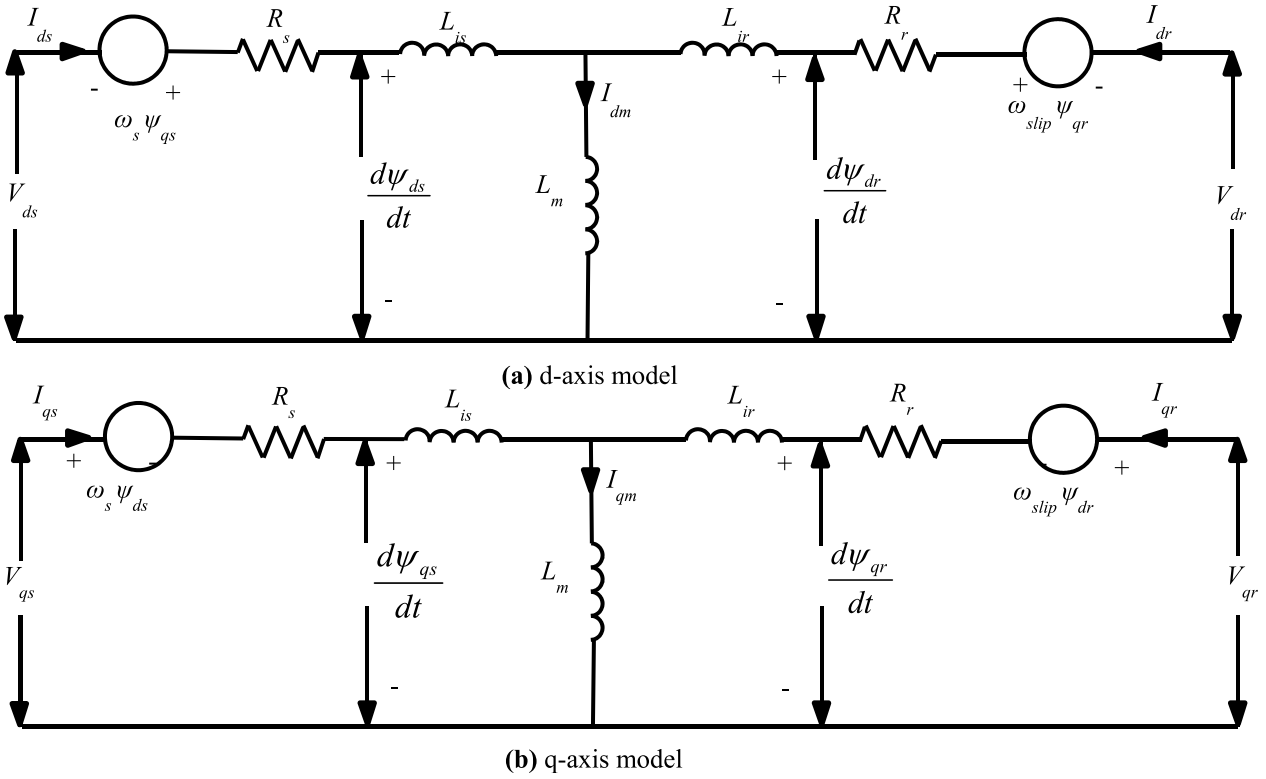

FIGURE 6. d-q axis mathematical model of DFIG.

Neglecting the stator resistance R_s [30], the stator active and reactive powers can be represented in terms of rotor current as follows:

$$P_s = -\frac{3}{2} V_{ds} \frac{L_m}{L_s} I_{dr} \tag{15}$$

$$Q_s = \frac{3}{2} V_{ds} - \left[\frac{V_{ds}}{\omega_s L_s} - \frac{L_m}{L_s} I_{qr} \right] \tag{16}$$

By rearranging (15) and (16), the following equations can be deducted:

$$I_{dr} = -\frac{2L_s}{3V_{ds}L_m} P_s \tag{17}$$

$$I_{qr} = -\frac{2L_s}{3V_{ds}L_m} Q_s - \frac{V_{ds}}{\omega_s L_m} \tag{18}$$

Owing to equations 17 and 18, the DFIG stator active power can be controlled by the tuning of the d-axis rotor current component whereas the q-axis current component controls the stator reactive power and the terminal voltage. In the proposed system, the DFIG RSC and GSC are mandated to carry out the control objectives for DFIG. Whereas, the RSC is responsible for regulating the stator terminal voltage to nominal level and prompting the DFIG to extract the maximum power from the available wind speed depending on tuning d-q axis components of the rotor current. The GSC is taking charge of regulating the DC link voltage and thus it would manage the power flow at GSC of DC link depending on the grid side d-q axis current components. Fig. 7 displays the SVO control scheme for both of GSC and RSC.

C. THE DG

The stochastic and intermittent characteristics of wind and solar powers necessitate the use of another power source that acts as a backup power source to cover the anticipated imbalance in load demand and guarantee the stability and reliability of the grid. DG system is considered one of the best selections to be integrated in a MG.

Although it is criticized for the expensive running cost of fossil fuel and the great environmental damage caused by generating green gases such as carbon dioxide, it is still marked by its large capacity, continuous power supply, strong environmental adaptability and flexible operating characteristics [31]. The DG system consists of two main parts. These are; a mechanical part comprising a diesel engine and a governor system that controls the output frequency and active power. The second part is electrical, consisting of a synchronous generator and an automatic voltage regulator (AVR) responsible for the terminal voltage regulation and the output reactive power.

Fig. 8 shows the schematic diagram of the considered synchronous generator. It is brushless type containing auxiliary synchronous called exciter mechanically coupled to the end of the main generator shaft. The main generator excitation coil is fed by a DC field current resulting from rectification of the AC output voltage of auxiliary exciter by diodes bridge mounted on the rotor. Adjusting the auxiliary exciter field current through the AVR, the generator output voltage is regulated [32].

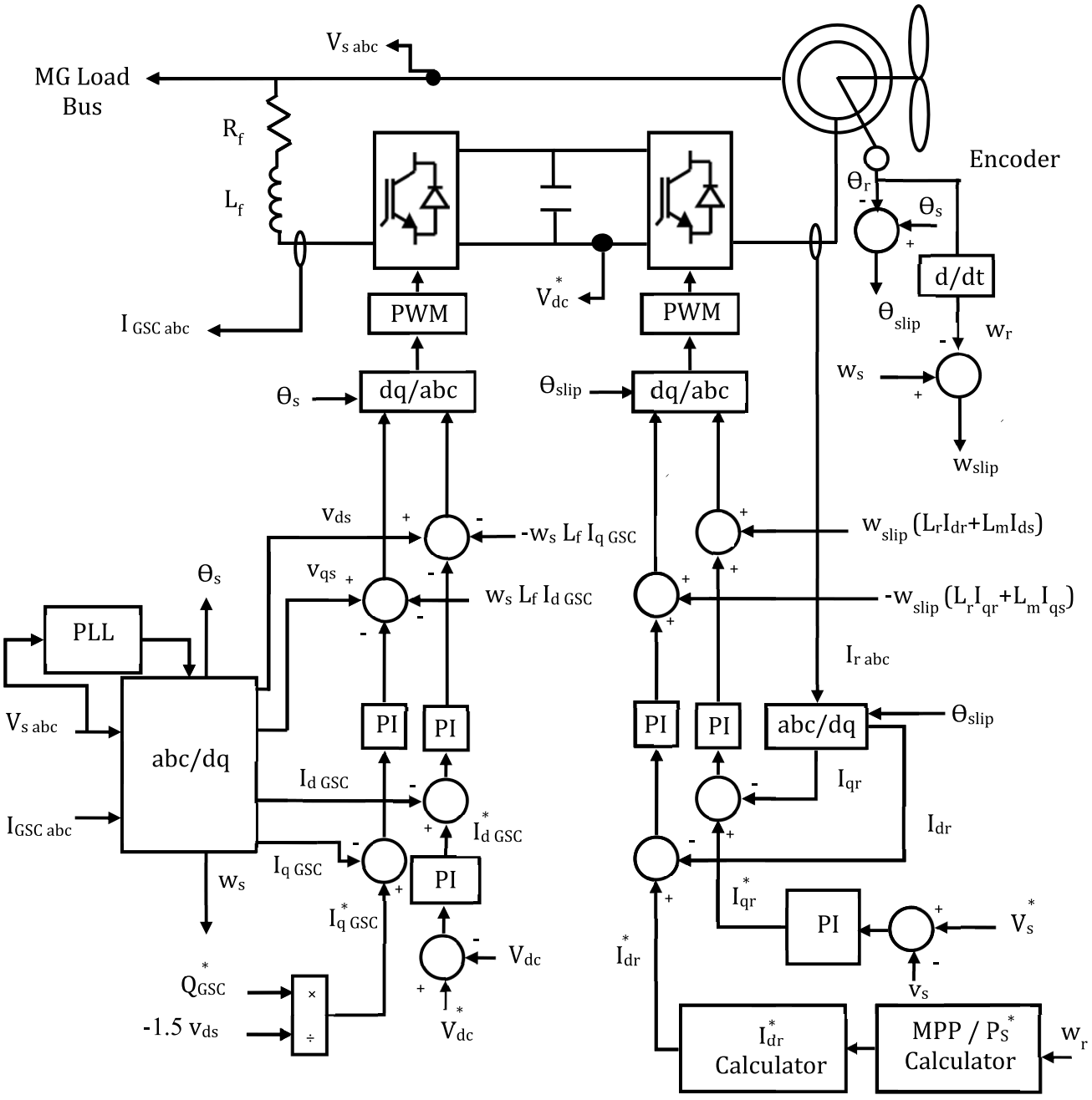

FIGURE 7. Stator voltage oriented (SVO) control schemes for DFIG GSC and RSC.

Table 5 displays the main technical specifications of the brushless synchronous generator used in this work. The selected rated output is asymptotic to the residential load so that the DG is able to supply the entire load in emergency situations.

III. RESULTS AND ANALYSIS

The proposed system is modeled and simulated using the MATLAB Simulink software package. Fig. 9 displays the simulated system structure. It contains three main controllers: WT controller, PV controller and ANFIS controller. The WT controller is meant to regulate both the DFIG stator and the GSC terminal voltages to always maintain 575 V as the main MG bus voltage. It also tunes the DC-link voltage and extracts the maximum power from the available wind. It uses signals from the DFIG stator voltage, stator current, rotor current, rotor angle, rotor speed, and DC-link voltage as inputs, whereas the outputs are the pulses to RSC and GSC.

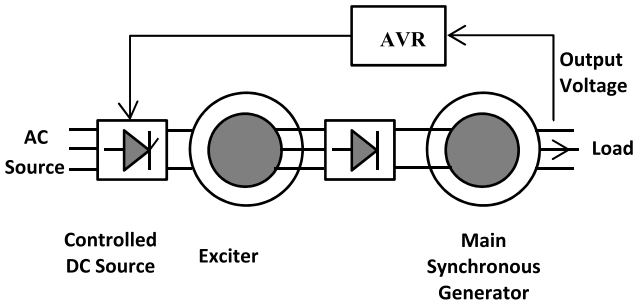

FIGURE 8. Typical architecture of brushless synchronous generators.

TABLE 5. The main technical specifications of the brushless synchronous generators.

Description	Specification
Rated apparent power	2 MVA
Rated speed	1500 rpm
Rated field current	2.25 A
Rated line-line voltage	400 V
Number of poles	4
Exciter apparent power	8.1 kVA
Rated frequency	50 Hz

The PV controller function is to extract the maximum power from the available irradiation. The inputs are voltage and current signals from PV terminals while the output is the pulses to boost converter gate. Lastly, the ANFIS controller is responsible for decreasing the fuel consumption of the DG to minimum level. The inputs and output of the ANFIS controller are explained before.

The proposed system performance with the ANFIS is initially evaluated under different climatic conditions simulating the daily natural weather fluctuations of solar irradiation, ambient temperature and wind speed. The solar irradiation reaches maximum in the morning then decreases until it fades away in night. Similarly, the ambient temperature rises to maximum during midday and falls to minimum during night. On the contrary, the wind speed is relatively low in daytime and increases gradually as the night falls. Moreover, the simulation has not overlooked the abrupt weather changes in which the wind speed may rise and the sky becomes gloomy, causing the irradiation and temperature to decrease as shown in patterns from period t=12 to 14 s.

To ensure the robustness of the proposed system, the step function is deliberately used in the changes of the three studied weather conditions. As displayed in Fig. 10(a), the wind speed is initially set at 12 m/s and starting from t=2 s, it decreases at a constant rate every two seconds until t=12 s. Then, there is a sudden increase from 7 to 10 m/s that stays constant for two seconds then decreases again to 7 m/s at t=14 s. After that, it increases again at a constant rate every two seconds until returning to 12 m/s at t=24 s.

The solar irradiation and ambient temperature are set initially at 0 W/m^2 and 15 c°, respectively. They are increased at a constant rate then decreased suddenly at t=12 s from 1000 W/m^2 and 40 c° to 600 W/m^2 and 30 c° for two seconds then re-increased to 1000 W/m^2 and 40 c° at t=14 s. They are decreased again at a constant rate until

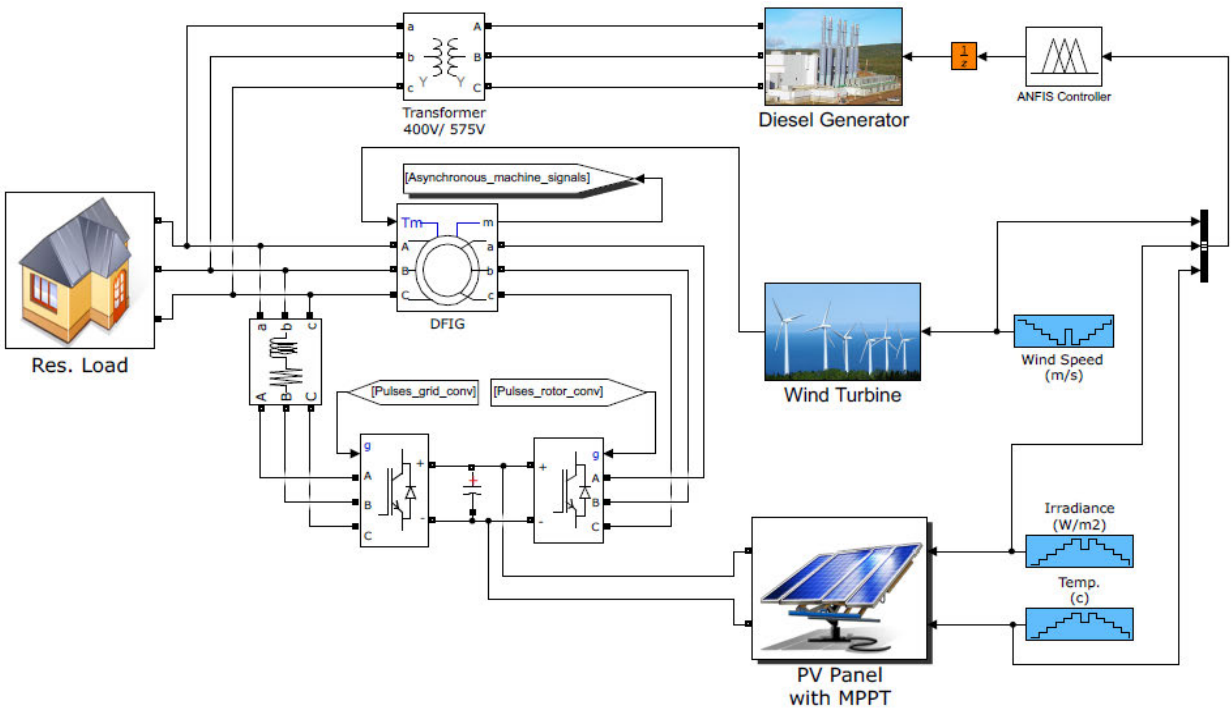

FIGURE 9. Simulink System Structure.

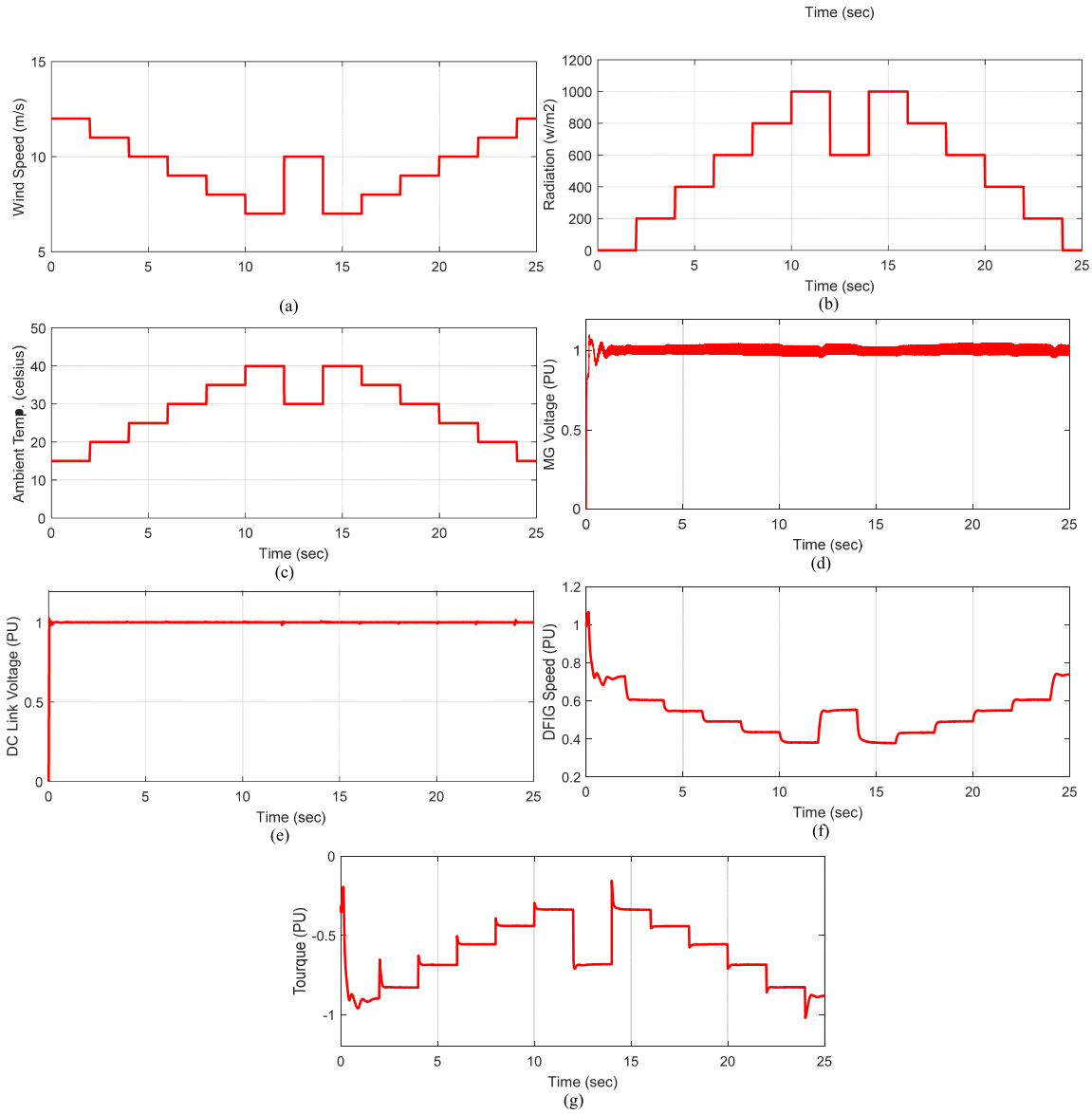

FIGURE 10. MG Response during variable weather conditions: (a) wind speed, (b) solar irradiation, (c) ambient temperature, (d) grid Voltage PU, (e) DC link voltage PU, (F) DFIG rotational speed, and (g) DFIG torque.

they are finally returned to 0 W/m^2 and 15 c°, as shown in Fig. 10(b) and 10(c).

The first objective of our PMS is to achieve the MG voltage stability. Fig. 10(d) shows the stator output voltage where it is remarked that the voltage is not affected by any changes in wind speed, irradiation or ambient temperature. The error is always kept within ± 5% of its rated voltage throughout the simulation period after system startup. In addition, the DC link bus voltage is within ± 2% error of its rated voltage as displayed in Fig. 10(e). Fig. 10(f) and Fig. 10(g) show the rotational speed and torque of the DFIG. As depicted from the figures, there is a relatively DFIG smooth running without overshooting even with different wind speed changes, except for the system startup time.

The power sharing between the different power sources in the proposed MG to supply the 2 MW residential load is illustrated in Fig. 11. The electrical and mechanical powers of the WT are displayed in Fig. 11(a) and 11(b), respectively. Fig. 11(c) shows the total power generated from the PV which completely or partially feeds the DC link according to the irradiation availability and the ambient temperature in day time. The DFIG stator output power is illustrated in Fig. 11(d) including both of the power generated from the wind and the power drawn from the DC link throughout the RSC shown in Fig. 11(e) irrespective of whether it comes from the PV or the GSC grid that acts as a bidirectional converter. The GSC supplies the DC bus partially or entirely in the event of lack or absence of the PV generated power. Whilst in the case of increased PV generated power, often due to high irradiation availability and high DFIG speeds, the excess power in the DC link drives the GSC to supply the grid instead, as shown in Fig. 11(f).

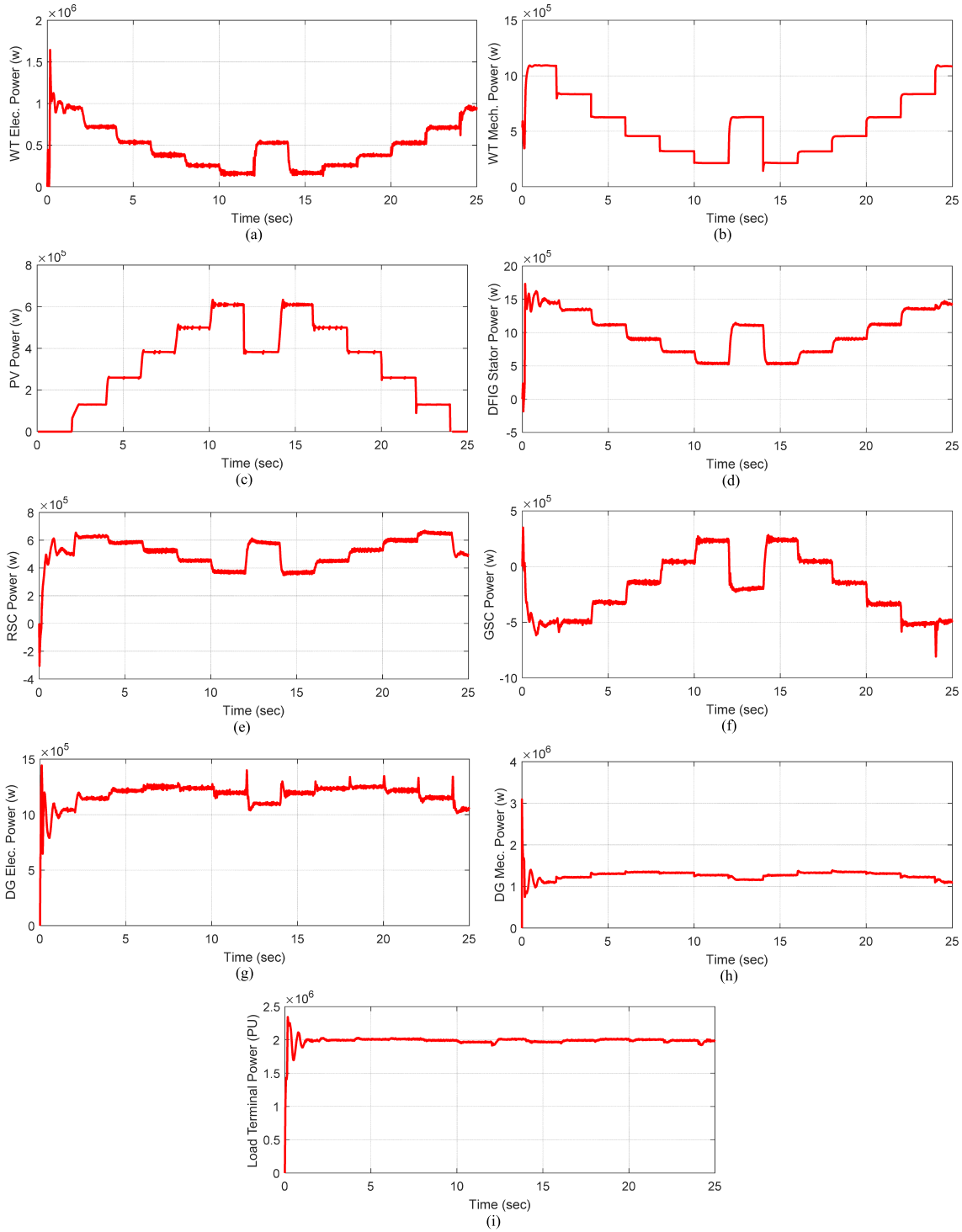

FIGURE 11. Power sharing of the different power sources in the proposed system: (a) wind turbine electrical power, (b) wind turbine mechanical power, (c) PV power, (d) DFIG stator power, (e) RSC power, (f) GSC power, (g) electrical DG power, (h) mechanical DG power, and (i) load power.

On the other hand, Fig. 11(g) displays the electrical power produced by the DG that resulted from the mechanical output power predicted by the ANFIS controller as shown in Fig. 11(h). Finally, Fig. 11(i) shows the total power supplying the residential load. It is proven from the figure that the proposed system has always been able to provide the required 2 MW power with error of no more than 2% achieving the desired power balance in the MG as the second objective of the work.

The MPP tracking of both the WT and PV is mandatory to reduce the consumption of the conventional fuel through minimizing the DG contribution to the system's power balance.

This covers the paper's third and fourth objectives that are almost achieved as displayed in Fig. 12 (a) and (b).

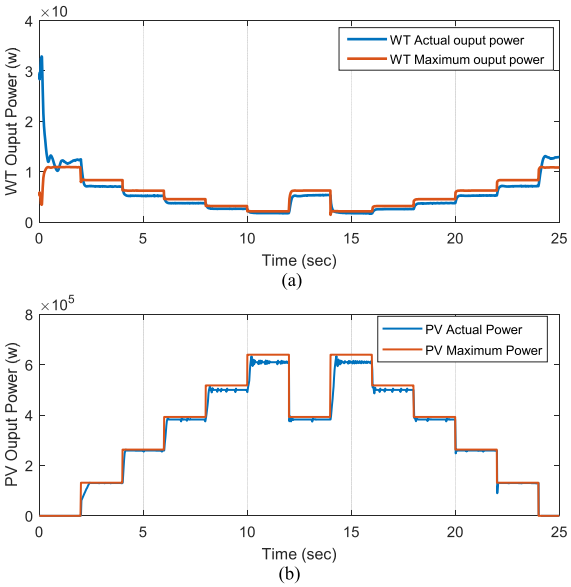

FIGURE 12. MPP tracking capability: (a) for the DFIG, (b) for the PV.

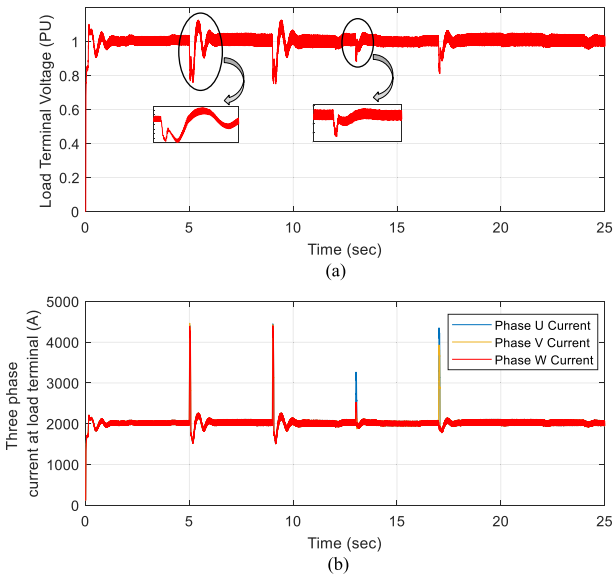

FIGURE 13. System Performance under different electrical faults at load terminal: (a) PU voltage stability, (b) the root mean square of the three phases fault current.

The proposed hybrid system and its ability to support the required loads should be checked, even in the event of any fault. Fig. 13 displays the system performance during exposure to different electrical faults at load terminals. The aforementioned faults include symmetrical and asymmetrical faults which occur and last for 50 m.s. Three phases to ground, three phases, single phase to ground and two phases faults occur at t = 5, 9, 13, 17 s., respectively.

Fig. 13(a) demonstrates the performance of the proposed system in restoring voltage stability at load terminal and returns to its nominal value after all electrical faults. The three phases to ground fault, being the last to reach the accepted

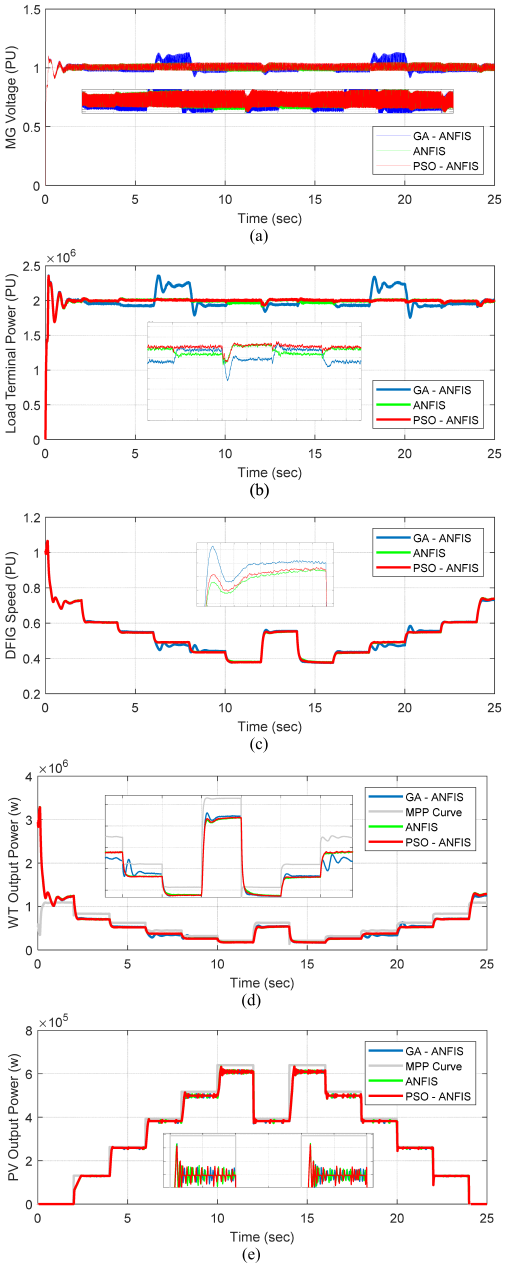

FIGURE 14. Comparison of the system performance during variable weather conditions using (GA-ANFIS), ANFIS and (PSO-ANFIS): (a) MG voltage PU, (b) Load Power, (c) DFIG speed, (d) PV MPP, (e) DFIG MPP.

stable voltage, takes 80 m.s. whereas the single phase to ground fault achieves stability after only 30 m.s. Fig. 13(b) shows the root mean square value of the three phases fault current at load terminal during the mentioned short circuit faults. The maximum short circuit current reaches 4460 A after three phases to ground fault and the minimum short circuit current reaches 3250 A after a single phase to ground fault.

Two different optimization algorithms are implemented as previously hinted. The results of (GA-ANFIS) and (PSO-ANFIS) are compared to those of ANFIS. Fig. 14 displays the comparative assessment of system performance

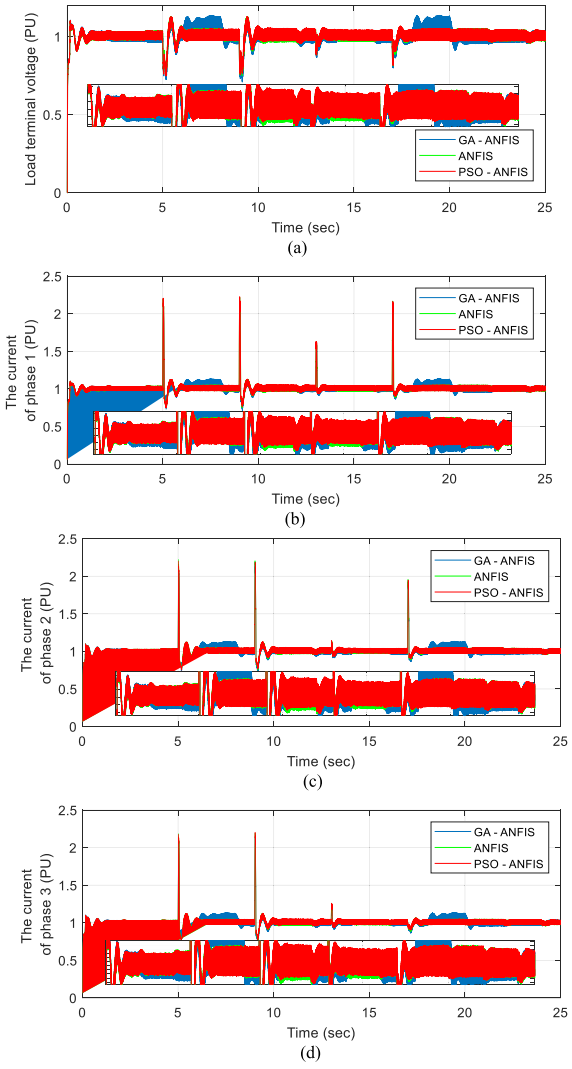

FIGURE 15. **Comparison of the system performance using (GA-ANFIS), ANFIS and (PSO-ANFIS) under different electrical faults at load terminal: (a) PU voltage stability, (b) & (c) and (d) the root mean square of the fault currents drawn in the three phases.**

in terms of load power, MG voltage, DFIG speed and MPP for both PV and WT. These are the five main criteria that can fully represent the efficiency of the system. In Figs. 14 (a) and (b), the MG voltage and load power stability with (PSO-ANFIS) are superior to that of ANFIS whose results are better than (GA-ANFIS). Both the (PSO-ANFIS) and (HLA-ANFIS) techniques provided smoother performance of the DFIG than that of (GA-ANFIS) as shown in Fig. 14 (c). In Figs. 14 (d) and (e), the MPP of PV and WT are almost similar for the three techniques. However, the curve of (GA-ANFIS) has sometimes exhibited over-shootings being higher or lower than that of (PSO-ANFIS) and ANFIS.

The system is further exposed to the same previously described electrical faults. The simulation results of (GA-ANFIS) and (PSO-ANFIS) are compared with those of ANFIS as shown in Fig 15. From the figure, it is concluded that the (PSO-ANFIS) has not only succeeded to restore the voltage stability after all the electrical faults but also it returned to the nominal value after only 70 m.s. with the three phases to ground fault and 25 m.s. with the single phase to ground fault, instead of 80 m.s. and 30 m.s. using the ANFIS. Whereas the (GA-ANFIS) has failed to restore the nominal voltage for the three phases to ground and two phases faults. Moreover, it has also failed to achieve satisfactory results for the other two faults compared to the ANFIS. The values of maximum and minimum three phases fault currents at load terminals for (GA-ANFIS), (PSO-ANFIS) are relatively the same as ANFIS as depicted in Fig. 15 (b), (c) and (d),

IV. CONCLUSION

A smart PMS based on ANFIS has been proposed for a MG constructed from hybrid renewable energy system composed of DFIG driven by WT and PV in conjunctions with DG. The GA and PSO optimization techniques have been employed in order to enhance the ANFIS parameters to achieve different objectives with different climatic and fault conditions. The results demonstrate that the proposed strategy is robust and could successfully achieve the voltage stability, balance the generated power and loads and track the MPP of the RERs. The superiority of the (PSO-ANFIS) is validated compared with the (GA-ANFIS) and the ANFIS. The MG with the proposed control strategy could successfully manage to achieve the required goals. The injected power from the RERs and DG is optimally shared by both the GSC and RSC in the proposed approach accommodating the uncertainty of the RERs.

REFERENCES

[1] A. Askarzadeh, "Electrical power generation by an optimised autonomous PV/wind/tidal/battery system," *IET Renew. Power Gener.*, vol. 11, no. 1, pp. 152–164, Jan. 2017.
[2] T. Ma and M. S. Javed, "Integrated sizing of hybrid PV-wind-battery system for remote island considering the saturation of each renewable energy resource," *Energy Convers. Manage.*, vol. 182, pp. 178–190, Feb. 2019.
[3] M. F. Zia, E. Elbouchikhi, and M. Benbouzid, "Microgrids energy management systems: A critical review on methods, solutions, and prospects," *Appl. Energy*, vol. 222, pp. 1033–1055, Jul. 2018.
[4] L. K. Gan, J. K. H. Shek, and M. A. Mueller, "Hybrid wind–photovoltaic–diesel–battery system sizing tool development using empirical approach, life-cycle cost and performance analysis: A case study in scotland," *Energy Convers. Manage.*, vol. 106, pp. 479–494, Dec. 2015.
[5] H. Lin, K. Sun, Z.-H. Tan, C. Liu, J. M. Guerrero, and J. C. Vasquez, "Adaptive protection combined with machine learning for microgrids," *IET Gener., Transmiss. Distrib.*, vol. 13, no. 6, pp. 770–779, Mar. 2019.
[6] Y. E. G. Vera, R. Dufo-López, and J. L. Bernal-Agustín, "Energy management in microgrids with renewable energy sources: A literature review," *Appl. Sci.*, vol. 9, no. 18, pp. 1–28, Sep. 2019.
[7] R. Bhaduri, G. R. Saravana, and C. Vaskar, "Supervisory controller for power management of microgrid using hybrid technique," *Trans. Electr. Electron. Mater.*, vol. 21, no. 1, pp. 30–47, Feb. 2020.
[8] S. Kewat, B. Singh, and I. Hussain, "Power management in PV-battery-hydro based standalone microgrid," *IET Renew. Power Gener.*, vol. 12, no. 4, pp. 391–398, Mar. 2018.
[9] J. Hong, J. Yin, Y. Liu, J. Peng, and H. Jiang, "Energy management and control strategy of photovoltaic/battery hybrid distributed power generation systems with an integrated three-port power converter," *IEEE Access*, vol. 7, pp. 82838–82847, 2019.
[10] P. S. Kumar, R. P. S. Chandrasena, V. Ramu, G. N. Srinivas, and K. V. S. M. Babu, "Energy management system for small scale hybrid wind solar battery based microgrid," *IEEE Access*, vol. 8, pp. 8336–8345, 2020.

[11] M. K. Senapati, C. Pradhan, S. R. Samantaray, and P. K. Nayak, "Improved power management control strategy for renewable energy-based DC micro-grid with energy storage integration," *IET Gener., Transmiss. Distrib.*, vol. 13, no. 6, pp. 838–849, Mar. 2019.
[12] S. Koohi-Kamali, N. A. Rahim, and H. Mokhlis, "Smart power management algorithm in microgrid consisting of photovoltaic, diesel, and battery storage plants considering variations in sunlight, temperature, and load," *Energy Convers. Manage.*, vol. 84, pp. 562–582, Aug. 2014.
[13] H. Razmi and H. Doagou-Mojarrad, "Comparative assessment of two different modes multi-objective optimal power management of micro-grid: Grid-connected and stand-alone," *IET Renew. Power Gener.*, vol. 13, no. 6, pp. 802–815, Apr. 2019.
[14] F. Valencia, J. Collado, D. Saez, and L. G. Marin, "Robust energy management system for a microgrid based on a fuzzy prediction interval model," *IEEE Trans. Smart Grid*, vol. 7, no. 3, pp. 1486–1494, May 2016.
[15] Y. K. Semero, J. Zhang, and D. Zheng, "EMD–PSO–ANFIS-based hybrid approach for short-term load forecasting in microgrids," *IET Gener., Transmiss. Distrib.*, vol. 14, no. 3, pp. 470–475, Feb. 2020.
[16] K. Basaran, N. S. Cetin, and S. Borekci, "Energy management for on-grid and off-grid wind/PV and battery hybrid systems," *IET Renew. Power Gener.*, vol. 11, no. 5, pp. 642–649, Apr. 2017.
[17] E. B. Ssekulima, M. B. Anwar, A. A. Hinai, and M. S. E. Moursi, "Smart energy management system for optimal microgrid economic operation," *IET Renew. Power Gener.*, vol. 10, no. 7, pp. 885–898, 2016.
[18] N. T. Mbungu, R. Naidoo, R. C. Bansal, and M. Bipath, "Optimisation of grid connected hybrid photovoltaic–wind–battery system using model predictive control design," *IET Renew. Power Gener.*, vol. 11, no. 14, pp. 1760–1768, Dec. 2017.
[19] S. Singh, M. Singh, and S. C. Kaushik, "Optimal power scheduling of renewable energy systems in microgrids using distributed energy storage system," *IET Renew. Power Gener.*, vol. 10, no. 9, pp. 1328–1339, Oct. 2016.
[20] I. M. Alarifi, H. M. Nguyen, A. N. Bakhtiyari, and A. Asadi, "Feasibility of ANFIS-PSO and ANFIS-GA models in predicting thermo-physical properties of Al_2O_3-MWCNT/oil hybrid nanofluid," *Materials*, vol. 12, no. 21, pp. 1–13, 2019.
[21] B. E. Elnaghi and S. A. Selim, "Performance of double fed induction generator based wind turbine using adaptive neuro-fuzzy inference system," in *Proc. IEEE Conf. Russian Young Researchers Electr. Electron. Eng. (EIConRus)*, St. Petersburg, Russia, Feb. 2017, pp. 808–813.
[22] N. Mahmud, A. Zahedi, and A. Mahmud, "A cooperative operation of novel PV inverter control scheme and storage energy management system based on ANFIS for voltage regulation of grid-tied PV system," *IEEE Trans. Ind. Informat.*, vol. 13, no. 5, pp. 2657–2668, Oct. 2017.
[23] S. Leonori, A. Rizzi, M. Paschero, and F. M. F. Mascioli, "Microgrid energy management by ANFIS supported by an ESN based prediction algorithm," in *Proc. Int. Joint Conf. Neural Netw. (IJCNN)*, Rio de Janeiro, Brazil, Jul. 2018, pp. 1–8.
[24] A. M. Kassem, "Modeling, analysis and neural MPPT control design of a PV generator powered DC motor-pump system," *WSEAS Trans. Syst.*, vol. 10, no. 12, pp. 399–412, Dec. 2011.
[25] G. Mamatha, "Perturb and observe MPPT algorithm implementation for PV applications," *Int. J. Comput. Sci. Inf. Technol.*, vol. 6, no. 2, pp. 1884–1887, 2015.
[26] R. Nair and G. Narayanan, "Emulation of wind turbine system using vector controlled induction motor drive," *IEEE Trans. Ind. Appl.*, vol. 56, no. 4, pp. 4124–4133, Aug. 2020.
[27] A. M. S. Yunus, A. Abu-Siada, M. A. S. Masoum, M. F. El-Naggar, and J. X. Jin, "Enhancement of DFIG LVRT capability during extreme short-wind gust events using SMES technology," *IEEE Access*, vol. 8, pp. 47264–47271, 2020.
[28] M. I. Mosaad, A. Alenany, and A. Abu-Siada, "Enhancing the performance of wind energy conversion systems using unified power flow controller," *IET Gener., Transmiss. Distrib.*, vol. 14, no. 10, pp. 1922–1929, May 2020.
[29] B. Subudhi and P. S. Ogeti, "Optimal preview stator voltage-oriented control of DFIG WECS," *IET Gener., Transmiss. Distrib.*, vol. 12, no. 4, pp. 1004–1013, Feb. 2018.
[30] B. Wu, Y. Lang, N. Zargari, and S. Kouro, *Power Conversion and Control of Wind Energy Systems*. Hoboken, NJ, USA: Wiley, 2011.
[31] B. Zhu, H. Tazvinga, and X. Xia, "Switched model predictive control for energy dispatching of a photovoltaic-diesel-battery hybrid power system," *IEEE Trans. Control Syst. Technol.*, vol. 23, no. 3, pp. 1229–1236, May 2015.
[32] M. Salah, K. Bacha, A. Chaari, and M. E. H. Benbouzid, "Brushless three-phase synchronous generator under rotating diode failure conditions," *IEEE Trans. Energy Convers.*, vol. 29, no. 3, pp. 594–601, Sep. 2014.

HESHAM M. FEKRY received the B.S. and M.S degrees in electrical power and machines engineering from Cairo University, Giza, Egypt, in 2006, and 2012, respectively. He currently works as the Electrical Section Head of Egyptian Propylene and Poly Propylene Company, which is considered one of biggest petrochemical plants in Middle East. His research interests include power system operation and management, renewable energy, generation and utilization electrical power, artificial intelligent in energy systems, power quality, micro-grid stability and control, smart grids, distributed generation, and AI applications in energy systems.

AZZA AHMED ELDESOUKY received the B.S. and the M.S degrees in electrical engineering from Suez Canal University, Port-Said, Egypt, in 1989, and 1995, respectively, and the Ph.D. degree from Bath University, U.K., in 2002. She is currently working as a Professor with the Department of Electrical Engineering, Port Said University. Her research interests include power system operation and management, power quality, microgrid stability and control, smart grids, distributed generation, and AI applications in energy systems.

AHMED M. KASSEM received the B.Sc. degree in electrical engineering from Assiut University, Egypt, in 1991, the M.Sc. degree in electrical engineering from Eindhoven Technical University, The Netherlands, in 1999, and the Ph.D. degree in electrical engineering from Minia University, Minia, Egypt, in 2006. He is currently a Professor of electrical power engineering with the Electrical Department, Faculty of Engineering, Sohag University, Egypt, where he has been the Dean of the Faculty of Engineering, since 2014. His research interests include smart energy grids, renewable energy management and control, energy storage, power electronics, power systems operation and control, renewable energy, electric drives and their control, electric vehicles, and storage energy development and intelligent control applications. He is an editorial board member for many journals and a consultant for many industrial companies and a peer reviewer in many transactions, periodicals, and conferences. He has supervised many Ph.D. and M.Sc. thesis and has published more than 70 research articles. He has got the Sohag University Superiority Award in 2018 in Engineering Sciences.

ALMOATAZ Y. ABDELAZIZ (Senior Member, IEEE) received the B.Sc. and M.Sc. degrees in electrical engineering from Ain Shams University, Cairo, Egypt, in 1985 and 1990, respectively, and the Ph.D. degree in electrical engineering according to the channel system between Ain Shams University, Egypt, and Brunel University, U.K., in 1996. He has been a Professor of electrical power engineering with Ain Shams University, since 2007. He is currently the Vice Dean of Faculty of Engineering and Technology, Future University in Egypt, Cairo, Egypt. He has authored or coauthored more than 400 refereed journal and conference papers, 25 book chapters, and three edited books with Elsevier and Springer. His research interests include the applications of artificial intelligence, evolutionary and heuristic optimization techniques to power system planning, operation, and control. He is a member of IET and the Egyptian Sub-Committees of IEC and CIGRE'. He has been awarded many prizes for distinct researches and for international publishing from Ain Shams University and Future University in Egypt. He is the Chairman of the IEEE Education Society chapter in Egypt. He is a Senior Editor of *Ain Shams Engineering Journal*, an Editor of *Electric Power Components and Systems Journal*, an editorial board member, an editor, an associate editor, and an editorial advisory board member for many international journals.